ABSTRACT

Title of Thesis: PIEZOELECTRIC ENERGY HARVESTING IN A SOFT SEGMENTED ROBOT

Nilanjana Ghosh
MS, 2021

Thesis Directed by: Dr. Derek A. Paley
Department of Aerospace Engineering and
Institute for Systems Research

The twenty-first century has seen a tremendous rise in electronic devices. However, this rise comes with a cost in energy. Researchers have been exploring alternate energy sources to replace traditional energy sources like batteries for the past two decades. Piezoelectricity is one of the less used alternate sources, which converts vibration energy into electricity. This thesis explores the energy harvested by piezoelectric devices from the movement of a soft robot. The energy harvested can recharge the power source that runs the robot. A model derived from the lumped-parameter model of piezoelectricity is developed for connected piezoelectric devices. This model is used to calculate the amount of energy generated from movements of the soft robot, like stretching and rotation. This thesis also highlights the stability and limitations of the proposed model.

PIEZOELECTRIC ENERGY HARVESTING IN A SOFT SEGMENTED ROBOT

by

Nilanjana Ghosh

Thesis submitted to the Faculty of the Graduate School of the
University of Maryland, College Park in partial fulfillment
of the requirements for the degree of
Master of Science
2021

Advisory Committee:
Dr. Derek A. Paley, Chair/Advisor
Dr. Miao Yu
Dr. Nikhil Chopra

Dedication

This work is dedicated to my parents Mr. Haru Ghosh and Mrs. Rinku Ghosh, to whom I owe everything that I have achieved till date

Acknowledgments

This thesis was made possible by several people to whom I will be grateful forever.

First and foremost, I would like to thank my advisor, Dr. Derek Paley, for giving me the opportunity to work on this project and making me a part of the Cooperative Dynamics and Control Lab. His constant guidance and advice made this thesis a reality. I would also like to thank Dr. Miao Yu and Dr. Nikhil Chopra for serving as committee members for this thesis. Finally, I would take up this opportunity to convey my thanks to Mr. Prateek Jaya Prakash and Dr. Will Scott, who built the background for this work.

I would also like to acknowledge Professor John Johnson and Dr. Michelle Bensi for hiring me as a graduate assistant and hence, helping me financially through graduate school. I would also like to thank all my professors at the Institute of Systems Research who helped me become a systems engineer.

I owe everything that I have achieved to my parents, Mr. Haru Ghosh and Mrs. Rinku Ghosh. Without their support, it would have been impossible for me to come this far. I would also like to mention my brother Mr. Anirban Ghosh, who was the bridge between my life in the USA and the one that I left in India. I would also like to thank my friends here at the University of Maryland and back home who motivated me to keep pushing through the trying times and not lose hope. I would like to specially mention Mr. Pratik Baneerjee for his constant support.

I would also like to extend my gratitude to the entire mental health community of the University of Maryland. They provided me the means to survive my graduate school life and helped me overcome my depression and anxiety.

Lastly, I would like to thank Google and MathWorks for providing me the technology to complete this project.

I apologize and extend my gratitude to everyone I could not mention here but who has been a part of my journey. Without you, this thesis would be incomplete.

Table of Contents

List of Figures

Chapter 1: Introduction

1.1 Motivation

Robotics has been the main focal point for most industries in the 21st century. With most industries transitioning to Industry 4.0, there has been a monumental rise in technologically advanced robots with higher degrees of computational power, capabilities, and precision. However, a drawback to these capabilities is the higher power requirement.

Traditional wireless power sources like electrochemical batteries require not only constant recharging but also affect the environment. To overcome these drawbacks, researchers are focusing on alternative energy sources for ambient energy harvesting. Ambient energy is available in the form of solar, thermal, or vibrational energy. One way to harvest vibrational energy is to use piezoelectric materials. Their inherent electromechanical coupling and high power density prove to be a good source for energy harvesting.

Though the piezoelectric effect was discovered in 1880, its use was limited to sensors and actuators. In the last few decades, with the increase in low power electronics, energy harvesting using piezoelectricity has become popular. However, extensive applications in this area are rare.

In robotic applications like soft robots, though the actuators are lightweight and flexible, they require rigid and heavy electronic and mechanical components to provide

power. Using heavy and rigid power sources reduces the flexibility and usage of a soft robot. To overcome this, energy harvested from the movement of a soft robot can be used to power it or extend its battery life.

This thesis explores the possibilities of using piezoelectric devices to generate energy from the movement of a soft segmented robot. The generated energy can be used to recharge the primary power source of the robot.

1.2 Literature Review

1.2.1 Piezoelectric Energy Harvesting

Certain materials can generate electric charges under applied stress. This phenomenon is known as the direct piezoelectric effect. However, these materials can also produce strain in response to an applied electric field. This phenomenon is known as the converse piezoelectric effect [1].

The piezoelectric effect has been used in high-precision actuation systems like micromanipulators, micro- valves, atomic force microscope, adaptive optics, ultra-precision machine tools, and structure dampers [2, 3]. Hence, the converse piezoelectric effect has seen several usages over the decades. However, using the direct piezoelectric effect, vibration energy can be converted to electrical energy. A rise in using the piezoelectric effect in recent years for energy harvesting can be attributed to the increase in low-power electronics [4]. Some popular applications of piezoelectric energy harvesting can be seen in harvesting mechanical energy from human motion [5] and harvesting energy from wind flows and water vertices [6, 7, 8].

Due to its high efficiency, simple structure, high voltage generation capability, and low cost, piezoelectric energy harvesting proves to be a good source of alternate energy technologies. In addition, the inherent electromechanical coupling of piezoelectric materials made it a popular choice over electromagnetic and electrostatic generators [9].

Piezoelectric energy harvesting is composed of three main parts: the energy source, the harvesting mechanism, and the energy sink [4, 10]. The energy source is the ambient source that produces the mechanical strain; it can be vibration due to movement or from environmental factors like wind. The harvesting mechanism refers to the electronic circuit used, and the energy sink can be a battery or a circuit that utilizes the generated voltage.

It is essential to develop a mathematical and analytical model of the energy harvesting technology to gain better insights into the system's function. Several models have been proposed for piezoelectric energy harvesting to describe the dynamics of the energy harvesting system. One of the more popular ones is the lumped parameter model [11, 12, 13]. This model provides a simple and efficient way to model the energy output from a piezoelectric device.

Naturally occurring piezoelectric materials are mostly crystals. However, developments in material science and manufacturing enable the construction of thin flexible and mechanically stretchable piezoelectric devices [14]. These material properties have increased the popularity of piezoelectric energy harvesting.

1.2.2 Motion of a Soft Robot

A soft robot is a robot made up of a soft appendage. Due to its flexible structure, it can be used for applications like underwater rescue missions, equipment maintenance, and surveillance, etc. [15]. Often a soft robot is discretized into a series of link or segments for analyzing its behavior [16, 17]. This provides a control problem involving many degrees of freedom, albeit fewer than a continuum model.

The locomotion of a snake-like robot is often defined using two main planar models: serpentine locomotion (horizontal locomotion) and traveling wave locomotion (vertical locomotion) [18, 19, 20].

A traveling wave is a spatiotemporal oscillation that is a periodic function of both space and time. The traveling wave locomotion describes the gaits of a snake-like robot [17]. A sinusoidal traveling wave equation shown in Equation 1.1 can be used to approximate the movement of a soft robot [20].

$$z = A \sin(\omega t + kx) \tag{1.1}$$

The travelling wave equation is used to describe the movement of the internal links of a soft segmented robot. The different modes of the movement of a snake like robot can be described using travelling wave equation described in Equation 1.1 [20].

1.3 Thesis Contribution

The primary contribution of this work is developing a model to calculate the voltage and power generated by piezoelectric devices from the movements of a soft segmented robot, like stretching and rotation. An analytical model for connected piezoelectric devices is derived from the lumped parameter model of piezoelectric energy harvesters [11, 13, 21].

The lumped parameter model provides a way to calculate the voltage generated by piezoelectric devices for a single piezoelectric structure. In this work, this model is expanded to multiple piezoelectric devices. In the proposed model, multiple piezoelectric devices are mechanically coupled with one another. Two main types of motion have been considered in this work: the stretching of a piezoelectric device and the rotation of connected piezoelectric devices. The model is simulated using external sinusoidal force and internal intrinsic length change.

The voltage generated and the stability of the model depend on parameters like electromechanical coupling factor and material parameters. These parameters have been extensively explored throughout this work.

1.4 Thesis Organization

Chapter 1 introduces the thesis and provides a brief overview of the previous works done on this topic. Chapter 2 outlines the mathematical and conceptual background for the thesis. Chapter 3 explores the behavior of piezoelectric devices when stretched.

The lumped parameter model introduced in Chapter 2 is used to derive the model for connected piezoelectric devices. Chapter 4 looks into the results of piezoelectric devices when rotated. Here, the lumped parameter model is used as a base to derive the models for rotation. Chapter 5 summarizes the results of this thesis and highlights the future direction of this work.

Chapter 2: Modeling of a Piezoelectric Energy Harvester

Piezoelectric Effect

The piezoelectric effect is the production of electric polarization by application of stress in certain solid materials [22]. It was first demonstrated by Pierre Curie and Jacques Curie in 1880.

The piezoelectric effect occurs as a result of charge distribution inside the material when stressed, as depicted in Figure 2.1. Due to charge redistribution in the material when stress is applied, an electric field will exist from the positive side to the negative side. The direction of the electric field will change when the applied stress is in the opposite direction.

As stated earlier, piezoelectric effect is divided into two major parts: the direct and the converse piezoelectric effects. When a piezoelectric material is mechanically strained, electric polarization proportional to the applied stress is produced. This effect is known as the direct piezoelectric effect. When the same material is subjected to an electric field, it becomes strained, and the amount of strain is proportional to the electric field. This effect is known as the converse piezoelectric effect [1]. The direct and converse piezoelectric effects can be represented as shown in Equation 2.1:

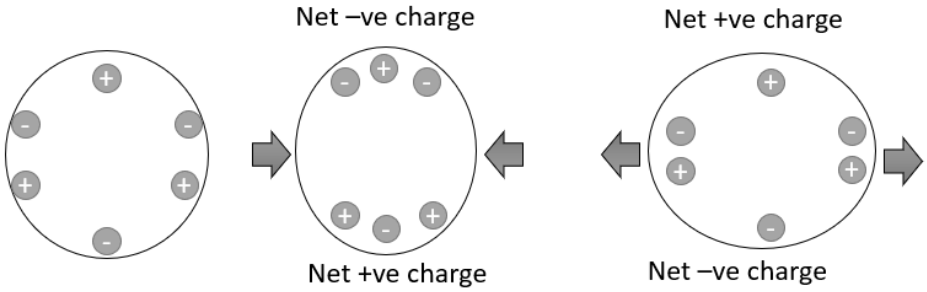

Figure 2.1: Redistribution of charge due to applied stress

$$\mathbf{P} = d\sigma \tag{2.1}$$

$$\mathcal{X} = d\mathbf{E} \tag{2.2}$$

Where, $\mathbf{P}$ is the polarization, σ is the stress applied, $\mathcal{X}$ is the strain produced, $\mathbf{E}$ is the electric field applied, and d is the piezoelectric coefficient.

We know that the polarization in a material is proportional to the electric field in the material, and the strain produced is proportional to stress, therefore [1, 4]:

$$\mathbf{P} = \epsilon\mathbf{E} \tag{2.3}$$

$$\mathcal{X} = s\sigma \tag{2.4}$$

Where, ϵ is the absolute permittivity of the material, and s is the material compliance.

We can combine the Equations 2.1 and 2.3 to get the coupled equations for piezoelectricity:

$$\begin{aligned} \mathbf{P} &= d\sigma + \epsilon\mathbf{E} \\ \mathcal{X} &= d\mathbf{E} + s\sigma \end{aligned} \tag{2.5}$$

The Equation 2.5 forms the basis of modeling of piezoelectric devices [1].

Lumped Parameter Model

A standard energy harvesting method for piezoelectricity is the cantilevered beam structure. An easy way to model the behavior of the cantilevered beam structure with a vibrating base is a spring-mass damper model [11, 23, 24]. A cantilevered bimorph beam is used as an energy harvester. Two oppositely polarized piezoelectric plates sandwiching the substrate are connected in series. A simple electrical circuit consisting of a load resistance R_L is connected to the output terminal of the harvester as shown in Figure 2.2.

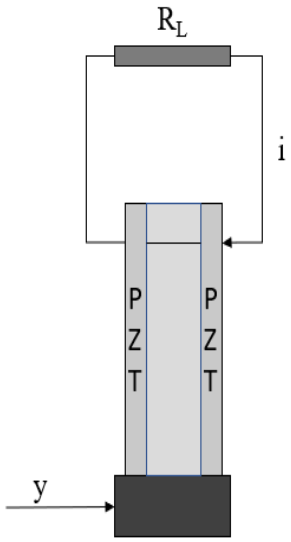

Figure 2.2: Cantilevered bimorph piezoelectric energy harvester

The harvester shown in Figure 2.2 can be modeled by using a mass-spring-damper model coupled with an electrical circuit as shown in Figure 2.3. Here, M is the equivalent mass, C and K are the equivalent damping and stiffness coefficient, respectively, C_P is the electrical capacitance formed, and y and x are the displacement of the base and the equivalent mass, respectively. In addition, an electromechanical coupling factor α exists between the mechanical and the electrical circuit.

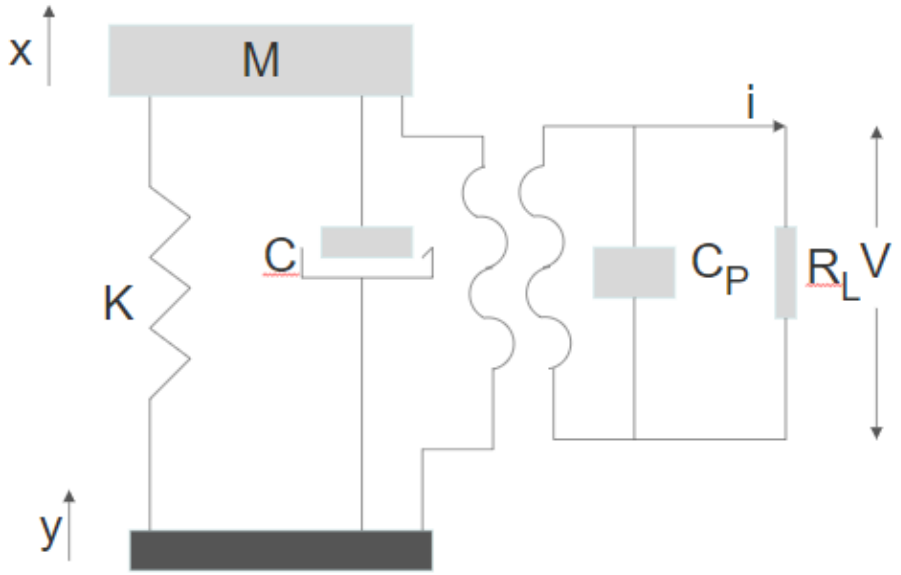

Figure 2.3: Single degree of freedom lumped-parameter model

The differential equation governing the equation of motion due to the vibrating base can be written as:

$$\begin{aligned} M\ddot{x} + B\dot{x} + Kx + \alpha V &= B\dot{y} + Ky \\ \alpha\left[\dot{x} - \dot{y}\right] - C\dot{V}(t) &= \frac{V}{R} \end{aligned} \tag{2.6}$$

The Equation 2.6 is used as a base to develop the models for piezoelectric energy harvesters with multiple degree of freedom.

Chapter 3: Energy Harvesting Incorporating Stretching

The lumped parameter model described in Section 2 is used to analyze the effects of stretching of a soft appendage. This chapter expands the model to multiple piezoelectric devices connected. A basic structure showing the stretching of a soft appendage is shown in Figure 3.1.

The responses of the model are derived for two types of forcing first, where external sinusoidal force is applied, and second when a traveling wave moves through the links.

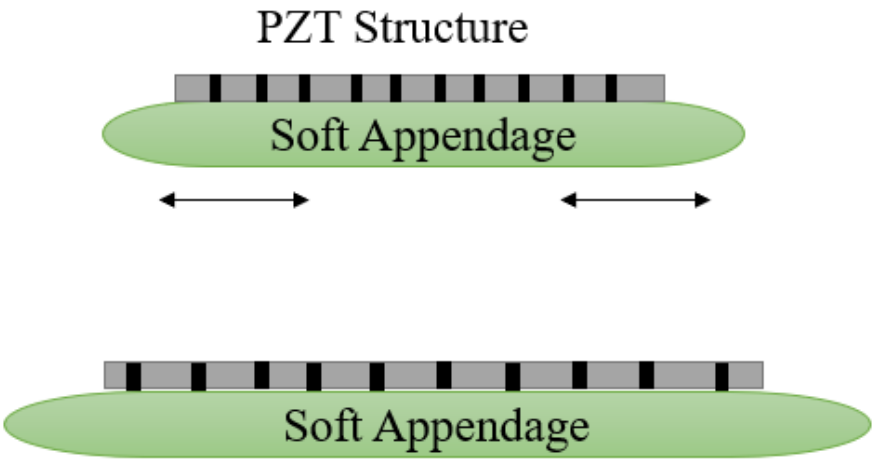

Figure 3.1: Stretching of a soft robot

3.1 Single Node Model

A state space model for the lumped parameter model defined in Section 2 is developed and used to analyze the voltage generated and the stability of the system.

3.1.1 Dynamic Modeling

From the Equation 2.6, we get the expressions for $\ddot{x}$ and $\dot{V}$ as follows:

$$\begin{aligned} \ddot{x} &= \frac{1}{M}\left(-B\dot{x} - Kx - \alpha V + B\dot{y} + Ky\right) \\ \dot{V} &= \frac{1}{C_P}\left(-\frac{V}{R_L} + \alpha\left[\dot{x} - \dot{y}\right]\right) \end{aligned} \tag{3.1}$$

Taking $\mathbf{z} = [x\ \dot{x}\ V]'$ to be the states of the system and input $\mathbf{u} = [y\ \dot{y}]'$ we get the state space equation as:

$$\begin{bmatrix} \dot{x} \\ \ddot{x} \\ \dot{V} \end{bmatrix} = \begin{bmatrix} 0 & 1 & 0 \\ -\frac{K}{M} & -\frac{B}{M} & -\frac{\alpha}{M} \\ 0 & \frac{\alpha}{C_p} & -\frac{1}{C_P R_L} \end{bmatrix} \begin{bmatrix} x \\ \dot{x} \\ V \end{bmatrix} + \begin{bmatrix} 0 & 0 \\ \frac{K}{M} & \frac{B}{M} \\ 0 & -\frac{\alpha}{C_P} \end{bmatrix} \begin{bmatrix} y \\ \dot{y} \end{bmatrix} \tag{3.2}$$

Integration of Equation 3.2 yields position of the lumped mass and the generated output voltage as shown in Figure 3.2.

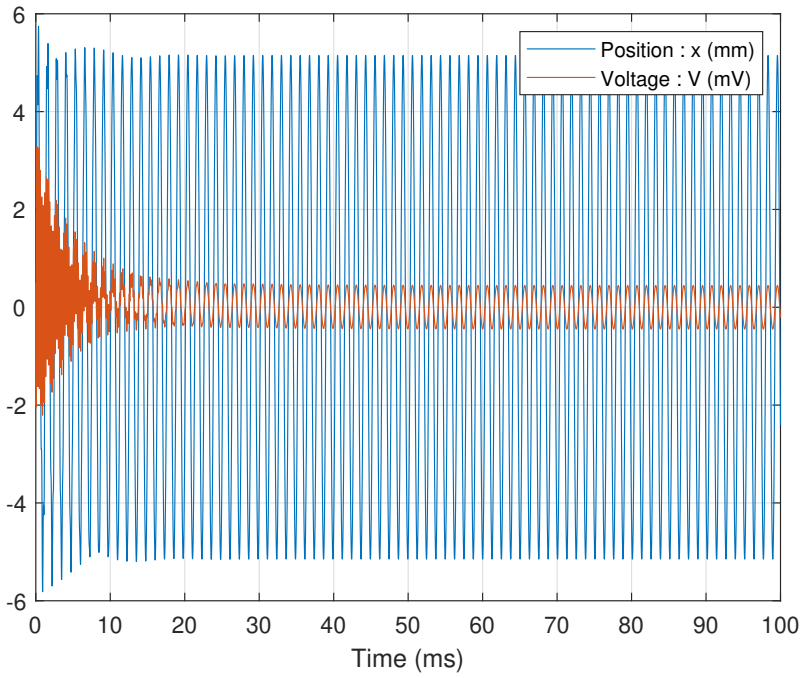

Figure 3.2: Position of mass vs. voltage generated for sinusoidal input

3.1.2 Stability Analysis

At zero input, i.e., when $\mathbf{u} = \mathbf{0}$ we have from Equation 3.2:

$$\dot{x} = \ddot{x} = 0$$

when

$$\frac{K}{M}x - \frac{\alpha}{M}V = 0 \tag{3.3}$$

and

$$\dot{V} = 0$$

when

$$-\frac{V}{C_P R_L} = 0 \tag{3.4}$$

From 3.3 and 3.4 we get, $\dot{z} = \mathbf{0}$ when $z = \mathbf{0}$. Again, from equation (3.2) with $\mathbf{u} = \mathbf{0}$ we get,

$$\dot{\mathbf{z}} = A\mathbf{z}$$

where

$$A = \begin{bmatrix} 0 & 1 & 0 \\ -\frac{K}{M} & -\frac{B}{M} & -\frac{\alpha}{M} \\ 0 & \frac{\alpha}{C_p} & -\frac{1}{C_p R_L} \end{bmatrix}$$

The eigen values of A are obtained from solving:

$$|A - \lambda I| = 0$$

Hence,

$$\begin{vmatrix} -\lambda & 1 & 0 \\ -\frac{K}{M} & -\frac{B}{M} - \lambda & -\frac{\alpha}{M} \\ 0 & \frac{\alpha}{C_p} & -\frac{1}{C_p R_L} \end{vmatrix} = 0$$

which implies

$$-\lambda \begin{vmatrix} -\frac{B}{M} - \lambda & -\frac{\alpha}{M} \\ \frac{\alpha}{C_p} & -\frac{1}{C_p R_L} - \lambda \end{vmatrix} - \begin{vmatrix} -\frac{K}{M} & -\frac{\alpha}{M} \\ 0 & -\frac{1}{C_p R_L} - \lambda \end{vmatrix} = 0$$

which implies

$$-\lambda \left(\left(-\frac{B}{M} - \lambda \right) \left(-\frac{1}{C_p R_L} - \lambda \right) + \frac{\alpha^2}{M C_p} \right) - \left(\frac{K}{M} \left(\frac{1}{C_p R_L} + \lambda \right) \right) = 0$$

which implies

$$\lambda^3 + \left(\frac{B}{M} + \frac{1}{C_p R_L} \right) \lambda^2 + \left(\frac{B}{M C_p R_L} + \frac{\alpha^2}{M C_p} + \frac{K}{M} \right) \lambda + \frac{K}{M C_p R_L} = 0 \tag{3.5}$$

$$\tag{3.6}$$

In 3.5 $B, M, C_p, R_L, \alpha > 0$, hence the coefficients of λ do not have any sign change. By Descartes' rule [25], we can conclude that no roots are in the right half of the plane. Hence, the origin of the system is exponentially stable.

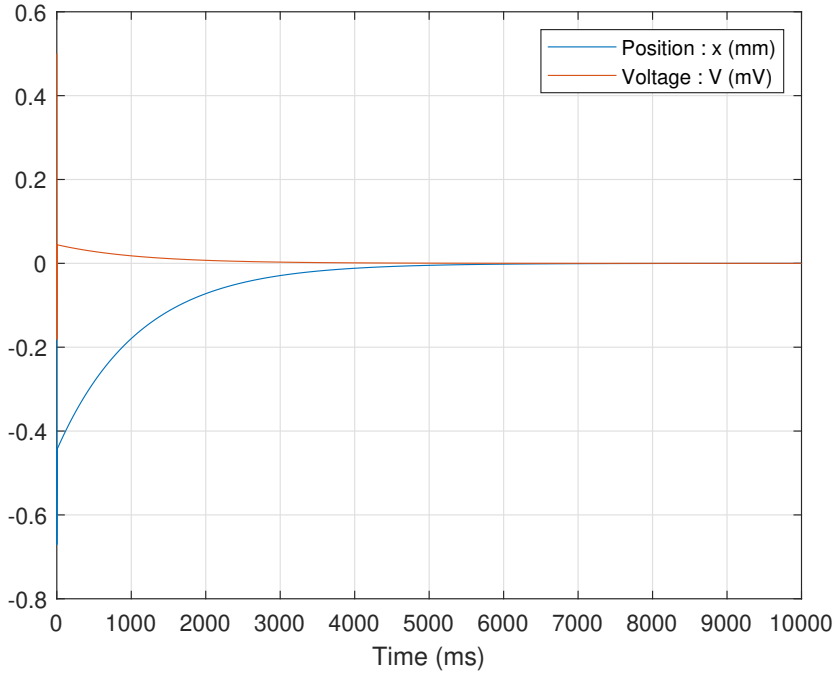

Figure 3.3: Steady state response of system 3.2

3.1.3 Energy Generated

The power output, P obtained from the piezoelectric device is proportional to the square of the voltage V^2, i.e.,

$$P = \frac{V^2}{R} \tag{3.7}$$

The output power when a sinusoidal input is applied to the single node piezoelectric device is shown in Figure 3.4 using $R = 100k\Omega$. The output power generated is in the range of microwatts.

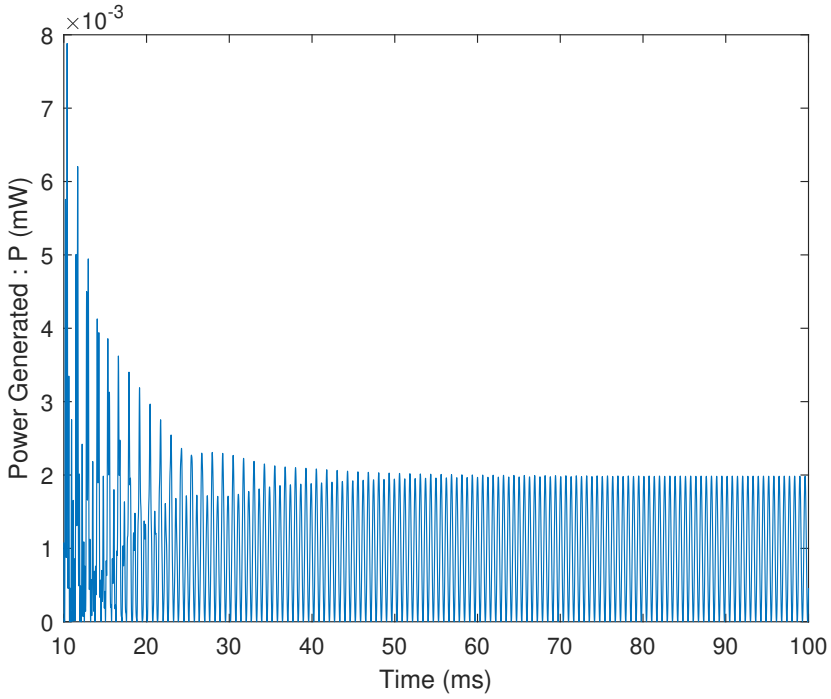

Figure 3.4: Electric power generated (P)

3.2 Multi Node Model

A soft robot can be represented as a continuum structure consisting of nodes and stretchable edges. To harvest energy from the movement of the soft robot, a structure similar to Figure 3.5 is suggested. Here, a piezoelectric device is attached to each node of soft robot. The output terminals of the piezoelectric devices are connected in series to get maximum voltage output.

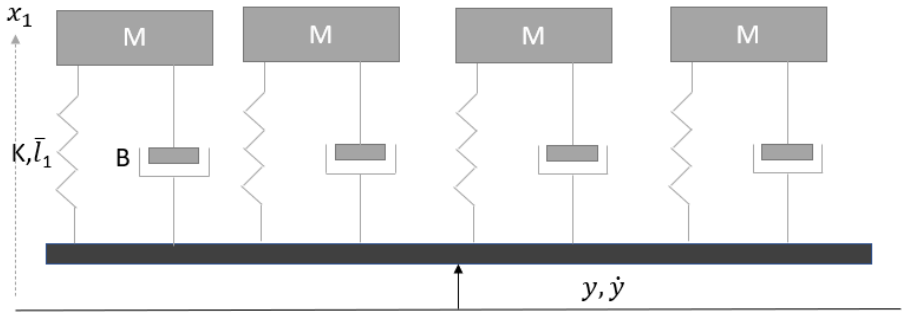

Figure 3.5: Multiple Lumped Piezoelectric Devices

The equations of motion for 3.5, for a n node system where $i = 1, 2, ..., n$ can be written as

$$\begin{aligned} M\ddot{x}_i + B\dot{x}_i + Kx_i + \alpha V_i &= B\dot{y}_i + Ky_i \\ \alpha\left[\dot{x}_i - \dot{y}_i\right] - C_{P_i}\dot{V}_i &= \frac{V_i}{R_i} \end{aligned} \tag{3.8}$$

The electrical parameters for series connected devices are given by

$$\begin{aligned} V_{eq} &= \sum_{i=1}^{i=n} V_i \\ \frac{1}{C_{Peq}} &= \sum_{i=1}^{i=n} \frac{1}{C_{P_i}} \\ R_{Peq} &= \sum_{1=1}^{i=n} R_i \end{aligned} \tag{3.9}$$

This model with a single vibrating base describes a system with vibrating only in

one direction, without any internal movements of the links. Thus, this model fails to describe the motion of a soft segmented robot.

3.2.1 Dynamic Modeling of Mechanically Coupled System

The links of a soft segmented robot is mechanically coupled together. Hence, in this section a mechanically coupled model of multiple piezoelectric devices is developed.

3.2.1.1 Modeling with Constant Intrinsic Length

A structure of multiple piezoelectric devices connected to one another can be devised as shown in Figure 3.6. The forces acting on the 1st, ith and nth mass is shown in Figure 3.7. The electrical output is connected in series to get maximum voltage.

Let $\bar{l}$ be the rest length of each spring. The length of the spring when the spring is stretched is

$$\begin{aligned} l_1 &= x_1 - y \\ l_i &= x_i - x_{i-1}, i = 2, \ldots, n \end{aligned} \tag{3.10}$$

To find the force produced by the stretching of spring, the difference between the stretched length and the intrinsic length is calculated:

$$\begin{aligned} \delta_1 &= l_1 - \bar{l}_1 = x_1 - \bar{l} - y \\ \delta_i &= l_i - \bar{l}_i = x_i - x_{i-1} - \bar{l} \end{aligned} \tag{3.11}$$

To get the rate of change of length the Equations 3.10 and 3.11 are differentiated with respect to time.

$$\begin{aligned} \dot{l}_1 &= \dot{x}_1 - \dot{y} \\ \dot{l}_i &= \dot{x}_i - \dot{x}_{i-1}, i = 2, \ldots, n \end{aligned} \tag{3.12}$$

$$\begin{aligned} \dot{\delta}_1 &= \dot{l}_1 - \dot{\bar{l}}_i = \dot{x}_1 - \dot{y} \\ \dot{\delta}_i &= \dot{l}_i - \dot{\bar{l}}_i = \dot{x}_i - \dot{x}_{i-1} \end{aligned} \tag{3.13}$$

Here $\dot{\bar{l}} = 0$ as $\bar{l}$ is constant.

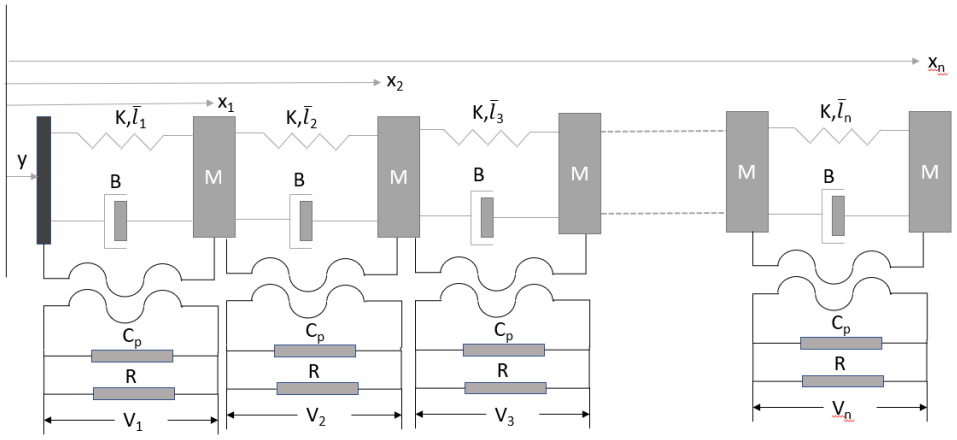

Figure 3.6: Connected Piezoelectric Devices

The forces acting on each node of the system in Figure 3.6 is shown in the free body diagram in Figure 3.7.

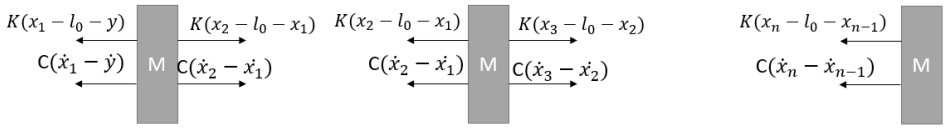

Figure 3.7: Forces acting on 1st, ith and nth node

The equations of motion of the for the multi node system in Figure 3.6 can be derived from the free body diagram in Figure 3.7. The force equations are:

$$\begin{aligned}
M\ddot{x}_1 &= -K\left(x_1 - \bar{l} - y\right) - B\left(\dot{x}_1 - \dot{y}\right) \\
&\quad + K\left(x_2 - \bar{l} - x_1\right) + B\left(\dot{x}_2 - \dot{x}_1\right) - \alpha V_1 \\
M\ddot{x}_i &= -K\left(x_i - \bar{l} - x_{i-1}\right) - B\left(\dot{x}_i - \dot{x}_{i-1}\right) \\
&\quad + K\left(x_{i+1} - \bar{l} - x_i\right) + B\left(\dot{x}_{i+1} - \dot{x}_i\right) - \alpha V_i \\
M\ddot{x}_n &= -K\left(x_n - \bar{l} - x_{n-1}\right) - B\left(\dot{x}_n - \dot{x}_{n-1}\right) - \alpha V \\
\alpha\left(\dot{x}_1 - \dot{y}_1\right) - C_P\dot{V}_1 &= \frac{V_1}{R} \\
\alpha\left(\dot{x}_{i+1} - \dot{x}_i\right) - C_P\dot{V}_i &= \frac{V_i}{R} \\
\alpha\left(\dot{x}_n - \dot{x}_{n-1}\right) - C_P\dot{V}_n &= \frac{V_n}{R}
\end{aligned} \tag{3.14}$$

The Equation 3.14 can be simplified to

$$
\begin{aligned}
M\ddot{x}_1 &= -2Kx_1 + Kx_2 - 2B\dot{x}_1 + B\dot{x}_2 - \alpha V_1 + Ky + B\dot{y} \\
M\ddot{x}_i &= -2Kx_i + Kx_{i+1} + Kx_{i-1} - 2B\dot{x}_i + B\dot{x}_{i+1} + B\dot{x}_{i-1} - \alpha V_i \\
M\ddot{x}_n &= -Kx_n + Kx_{n-1} + K\bar{l} - B\dot{x}_n + B\dot{x}_{n-1} - \alpha V_n \\
C_P\dot{V}_1 &= -\alpha\left(\dot{x}_1 - \dot{y}\right) - \frac{V_1}{R} \\
C_P\dot{V}_i &= -\alpha\left(\dot{x}_i - \dot{x}_{i-1}\right) - \frac{V_i}{R}
\end{aligned}
\tag{3.15}
$$

The overall voltage generated by the piezoelectric structure when connected in series is given by Equation 3.9.

3.2.1.2 Modeling with Varying Intrinsic Length

For a travelling wave through the stacked piezoelectric material, each of the links will expand and contract according to the dynamics of the travelling wave. In this scenario the intrinsic length of the spring $\bar{l}_i$ constantly changes. If a wave $\bar{l}_i$ travels through the links then we have the following equations:

$$
\bar{l}_i = \bar{l}_0 + l_0 \sin\left(\omega t + \phi_i\right) \tag{3.16}
$$

The equations of motion from Equation 3.15 can be modified to include the varying intrinsic length as

$$
\begin{aligned}
M\ddot{x}_1 &= -K\left(x_1 - \bar{l}_1 - y\right) - B\left(\dot{x}_1 - \dot{l}_1 - \dot{y}\right) \\
&\quad + K\left(x_2 - \bar{l}_2 - x_1\right) + B\left(\dot{x}_2 - \dot{l}_2 - \dot{x}_1\right) - \alpha V_1 \\
M\ddot{x}_i &= -K\left(x_i - \bar{l}_i - x_{i-1}\right) - B\left(\dot{x}_i - \dot{l}_i - \dot{x}_{i-1}\right) \\
&\quad + K\left(x_{i+1} - \bar{l}_{i+1} - x_i\right) + B\left(\dot{x}_{i+1} - \dot{l}_{i+1} - \dot{x}_i\right) - \alpha V_i \\
M\ddot{x}_n &= -K\left(x_n - \bar{l}_n - x_{n-1}\right) - B\left(\dot{x}_n - \dot{l}_n - \dot{x}_{n-1}\right) - \alpha V_2 \\
\alpha\left[\dot{x}_1 - \dot{l}_1 - \dot{y}_1\right] - C_P\dot{V}_1 &= \frac{V_1}{R} \\
\alpha\left[\dot{x}_i - \dot{l}_i - \dot{x}_{i-1}\right] - C_P\dot{V}_i &= \frac{V_i}{R} \\
\alpha\left[\dot{x}_n - \dot{l}_n - \dot{x}_{n-1}\right] - C_P\dot{V}_n &= \frac{V_n}{R}
\end{aligned}
\tag{3.17}
$$

The Equation 3.17 can be simplified to

$$
\begin{aligned}
M\ddot{x}_1 &= -2Kx_1 + Kx_2 + K\bar{l}_1 - K\bar{l}_2 - 2B\dot{x}_1 + B\dot{x}_2 + B\dot{\bar{l}}_1 - B\dot{\bar{l}}_2 - \alpha V_1 + Ky + B\dot{y} \\
M\ddot{x}_i &= -2Kx_i + Kx_{i+1} + Kx_{i-1} + K\bar{l}_i - K\bar{l}_{i+1} + 2B\dot{x}_i + B\dot{x}_{i+1} + B\dot{x}_{i-1} - B\dot{\bar{l}}_{i+1} + B\dot{\bar{l}}_i - \alpha V_i \\
M\ddot{x}_n &= -Kx_n + Kx_{n-1} + K\bar{l}_n - B\dot{x}_n + B\dot{x}_{n-1} + B\dot{\bar{l}}_n - \alpha V_n \\
C_P\dot{V}_1 &= -\alpha\left[\dot{x}_1 - \dot{\bar{l}}_1 - \dot{y}_1\right] - \frac{V_1}{R} \\
C_P\dot{V}_i &= -\alpha\left[\dot{x}_{i+1} - \dot{\bar{l}}_i - \dot{x}_i\right] - \frac{V_i}{R}
\end{aligned}
\tag{3.18}
$$

3.2.2 Stability Analysis

The system of Equation, 3.15 and 3.18 are unstable for certain values of α, K and B only. To analyse this phenomenon, the damping coefficient ζ is defined as

$$\zeta = \frac{B}{2\sqrt{KM}} \tag{3.19}$$

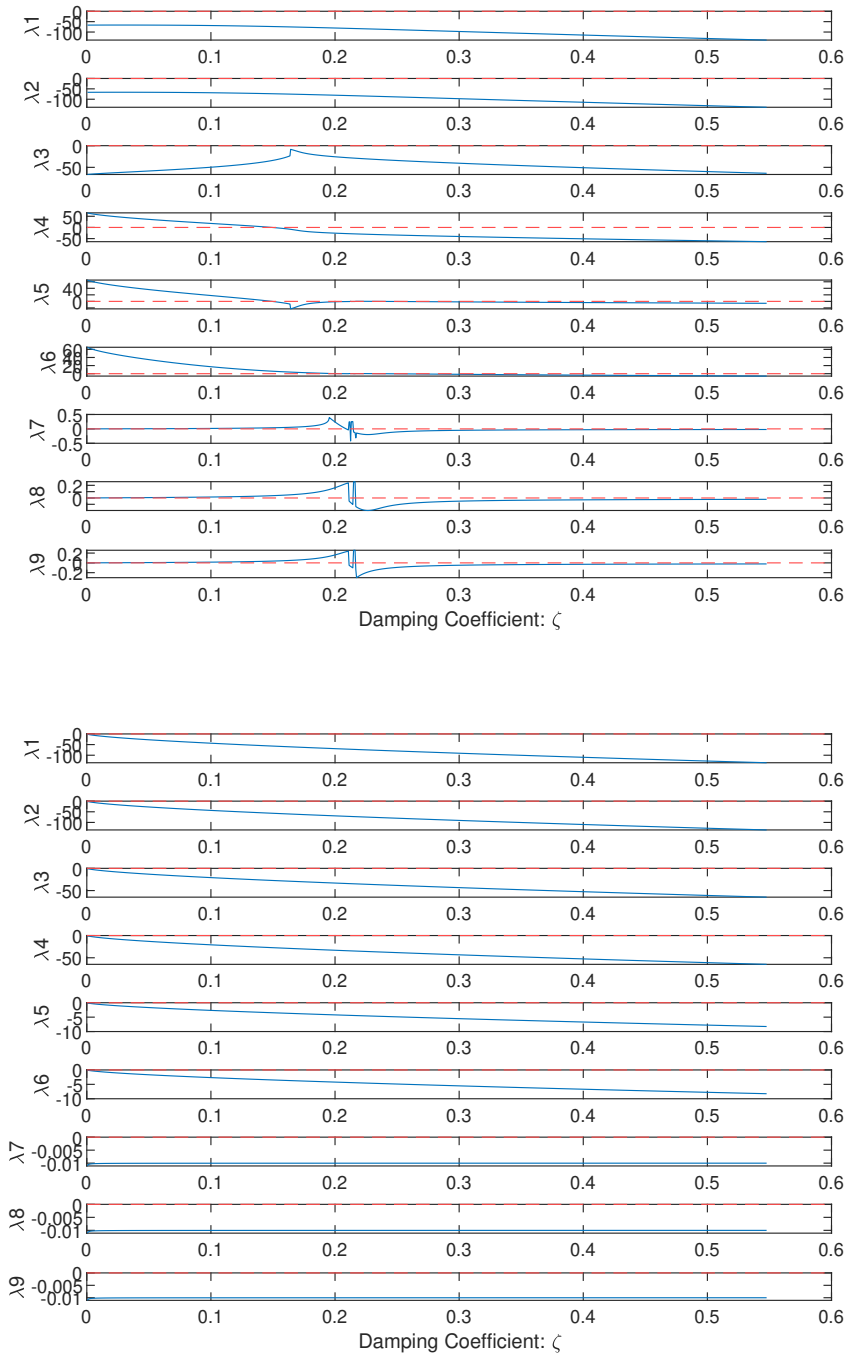

Figure 3.8: Bifurcation Diagram for different values of $\alpha = 7.3$ and 0.3 and varying ζ

It can be observed from Figure 3.8 that the real part of the eigenvalues λ becomes

positive at certain values of K and B. The system becomes unstable at these values. It is observed that the system is stable for lower values of the coupling factor α. At the values for which the system becomes unstable, the length of the soft appendage increases indefinitely and the voltage also increases proportionally.

3.2.3 Model Response for Different Forcing

The models developed in Sec. 3.2.1.1 and 3.2.1.2, are simulated with sinusoidal inputs. This section focuses on the responses for the models for the different inputs.

3.2.3.1 Responses for Constant Intrinsic Length

The model defined in 3.2.1.1 is given a sinusoidal input $\mathbf{u} = [a\sin(\omega t)\ \ a\omega\cos(\omega t)]^{'}$, where $a = 5$ and $\omega = 5$. The system is simulated for 3 and 10 nodes respectively, as shown in Fig. 3.9 and 3.10. The position, x and voltage, V both have initial conditions.

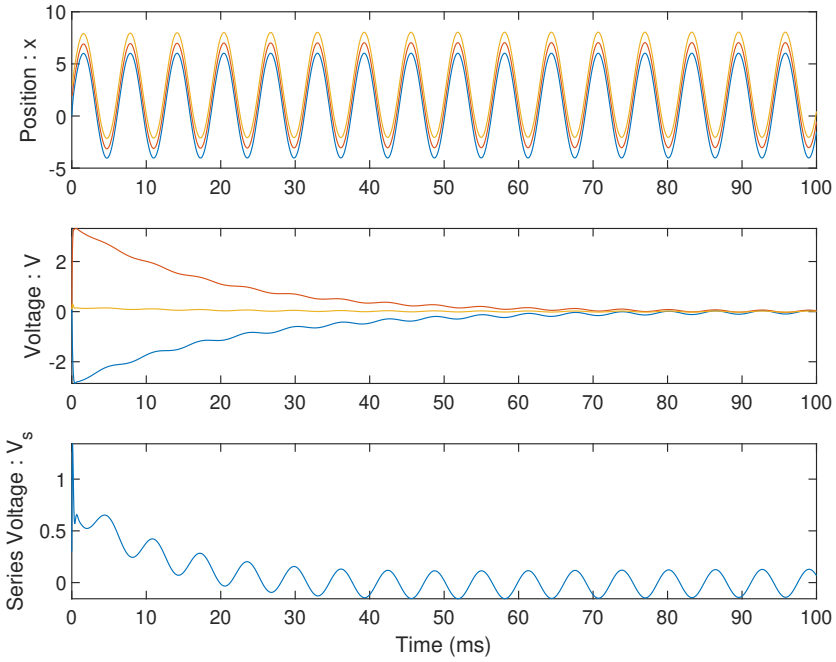

Figure 3.9: Position and voltage for stretching in 3 nodes

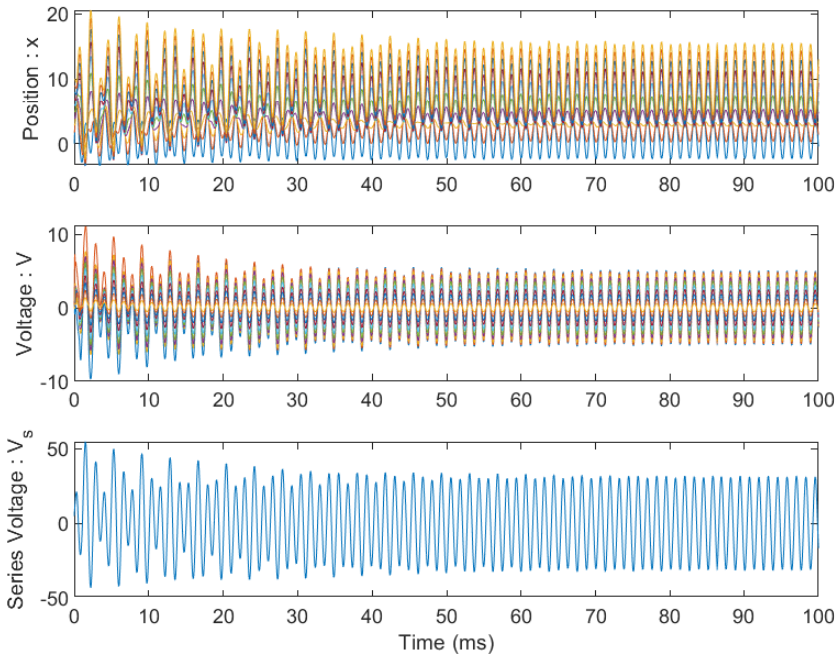

Figure 3.10: Position and voltage for stretching in 10 nodes

When starting from a higher initial condition, the voltage takes some time to stabilize and give a sinusoidal output. Increasing the number of nodes, means increasing the number of piezoelectric devices, hence, it can be seen that increasing the number of nodes, keeping the model and input parameters constant, gives a higher series voltage, V_s. Also, with the increase in number of nodes, the system takes longer time to give a steady voltage output.

3.2.3.2 Response for Varying Intrinsic Length

The model defined in Sec. 3.2.1.2 is given a sinusoidal input $\mathbf{u} = [a\sin(\omega t) \;\; a\omega\cos(\omega t)]'$. The model is simulated with $a = 5$ and $\omega = 5$, with $\bar{l} = 0.1mm$. The response of the

model is for 3 nodes, and 10 nodes can be seen in Fig. 3.11 and Fig. 3.12 respectively.

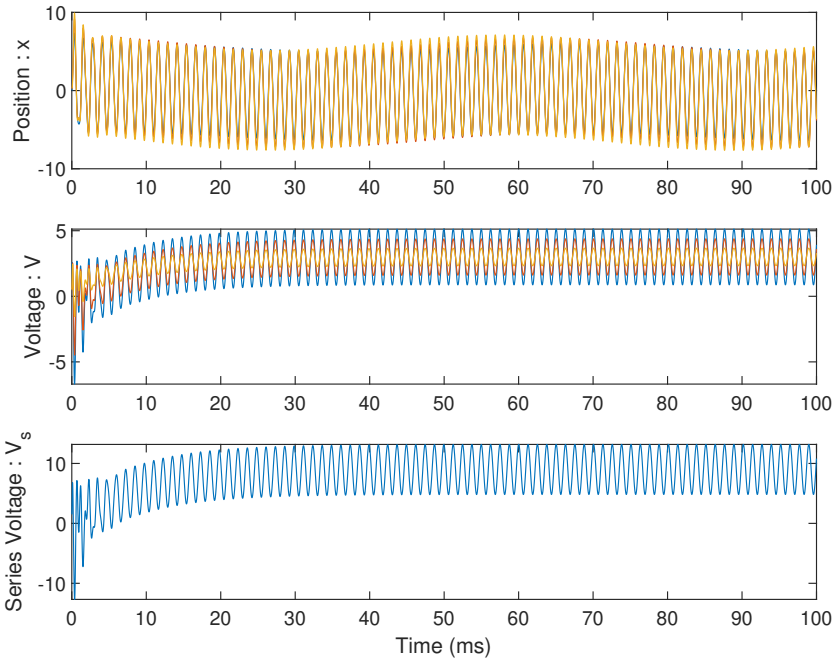

Figure 3.11: Position and voltage for stretching in 3 nodes with travelling wave

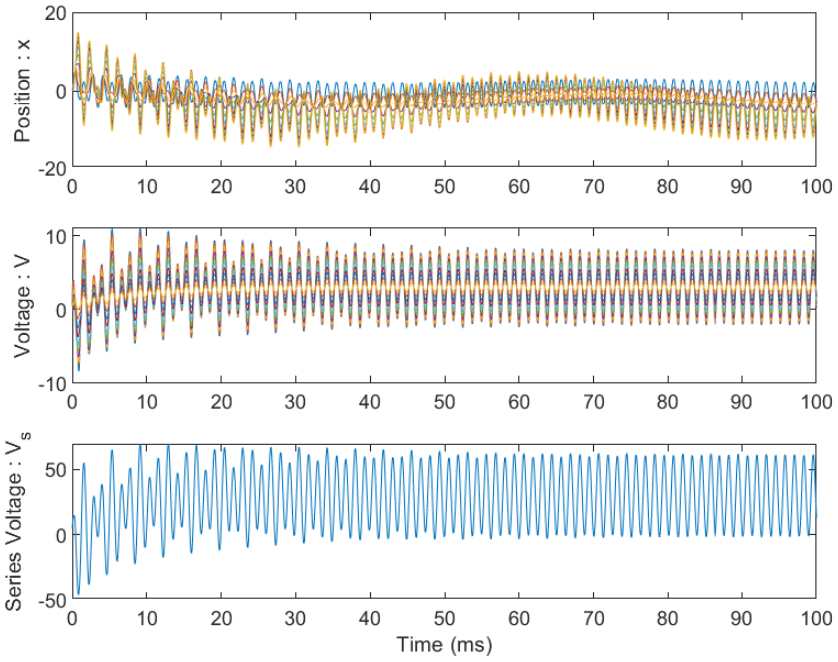

Figure 3.12: Position and voltage for stretching in 10 nodes with travelling wave

In this case, when the internal length between each node changes in accordance to a travelling wave equation, the position of each node, hence, the output voltage generated is out of phase from one another. As the voltages are out of phase, thus, the resultant series voltage does not cancel each other, hence, we get a higher voltage output. Moreover, the stress generated due to change in intrinsic length also contributes to the output voltage.

3.2.4 Energy Generated

The power output in the multi node case is similar to the power output defined for single node case. For multiple piezoelectric devices connected in series can be defined as:

$$P = \frac{\sum_{i=1}^{n} V_i^2}{R} \tag{3.20}$$

The output power for stretching with constant and varying intrinsic length can be seen in Fig. 3.13 and 3.14. As seen in the case of generated voltage, the output power is higher for varying intrinsic length rather than constant intrinsic length.

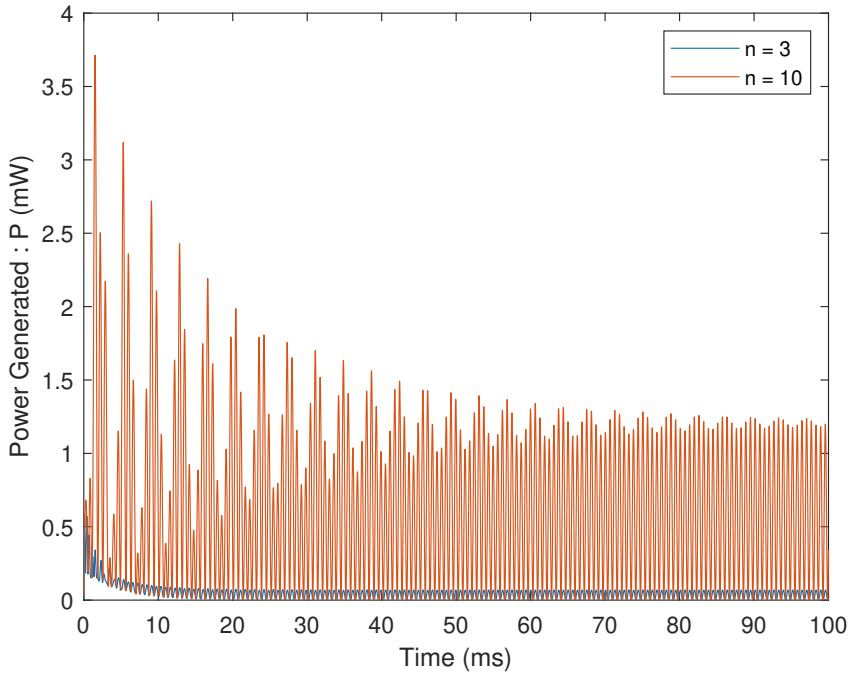

Figure 3.13: Power generated for 3 nodes and 10 nodes respectively in constant intrinsic length

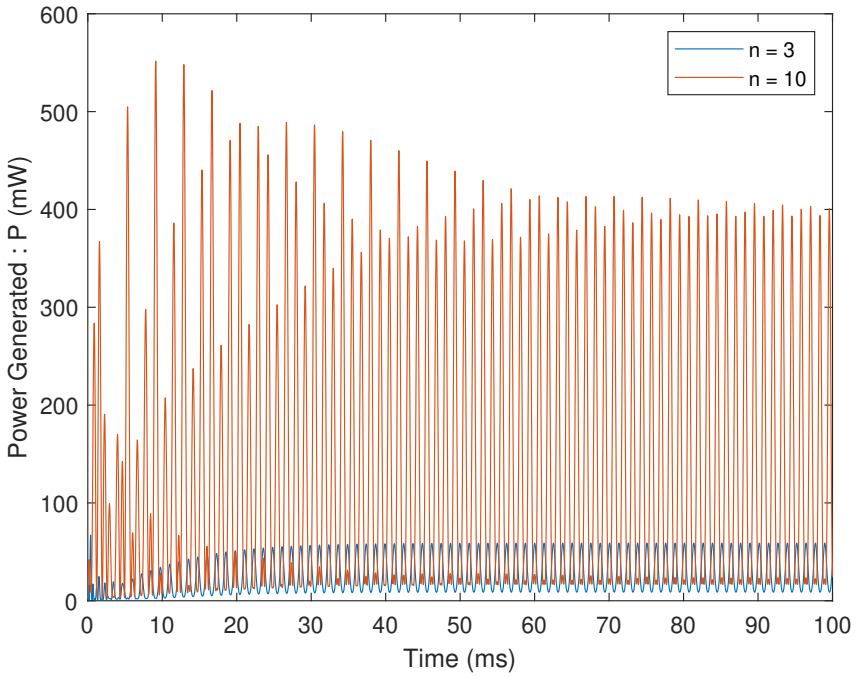

Figure 3.14: Power generated for 3 nodes and 10 nodes respectively in varying intrinsic length

Chapter 4: Energy Harvesting Incorporating Rotation

This chapter expands the concepts from Chapter 3 to rotation of a piezoelectric device. Here, the piezoelectric devices are modeled as rigid rods rotating around the origin with spring and damper attached in between. The input vibrating force is applied at the tip of the rod away from the origin.

4.1 Single Node Model

The single node model is shown in Fig. 4.1. It consists of a base rod, which rotates with an input $u = \begin{bmatrix} \phi & \dot{\phi} \end{bmatrix}$. Another rod, that rotates at an angle θ as a response to the input. The length of the spring $\bar{l}$ between each rod can be defined as:

$$\bar{l} = r\left(\bar{\theta}\right) \tag{4.1}$$

Where $\bar{\theta}$ is the intrinsic rotating angle.

4.1.1 Dynamic Modeling

For rotating motion, we consider the spring in between each node, with rotational spring constant κ and damping of $\mathcal{B}$, bends by an angle θ. The motion of the system is

shown in 4.1. Assume that the nodes are equally spaced from the origin, hence, $r_0 = r_1 = r$.

The translational velocity of the first node with respect to the base node is

$$\begin{aligned} \mathbf{v_1} - \mathbf{v_0} &= r_1\dot{\theta} - r_0\dot{\phi} \\ \mathbf{v_1} - \mathbf{v_0} &= r\left(\dot{\theta} - \dot{\phi}\right) \end{aligned} \tag{4.2}$$

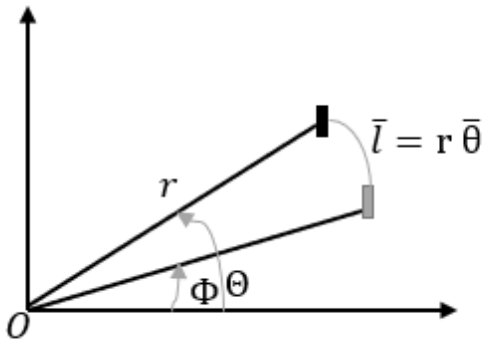

Figure 4.1: Single Node Bending

For the system in Equation 4.1 the equations of motion are:

$$\begin{aligned} I\ddot{\theta} = -\kappa \sin\left(\theta - \bar{\theta} - \phi\right) - \mathcal{B}\left(\dot{\theta} - \dot{\phi}\right) - \alpha V \\ \alpha r\left(\dot{\theta} - \dot{\phi}\right) - C_p\dot{V} = \frac{V}{R} \end{aligned} \tag{4.3}$$

If the angles, $\theta, \bar{\theta}, \phi$ are sufficiently small. Hence, using the small angle approximation yields:

$$\begin{aligned}\ddot{\theta} &= \frac{1}{I}\left(-\kappa\theta - \kappa\bar{\theta} - \mathcal{B}\dot{\theta} - \alpha V + \kappa\phi + \mathcal{B}\dot{\phi}\right) \\ \dot{V} &= \frac{1}{C_p}\left(\alpha r\left(\dot{\theta} - \dot{\phi}\right) - \frac{V}{R}\right)\end{aligned} \tag{4.4}$$

In Equations 4.3 and 4.4, $I = Mr^2/3$.

4.1.2 Voltage and Energy Response

The single node model defined in the previous section is simulated using sinusoidal input. The voltage generated from the rotation of the piezoelectric device is shown in Fig. 4.2 and Fig. 4.3 shows the corresponding power generated. The voltage generated after stabilization is very low compared to the stretching scenario as the amount of strain produced in rotation is smaller. The output power of the system is given by Equation 3.7.

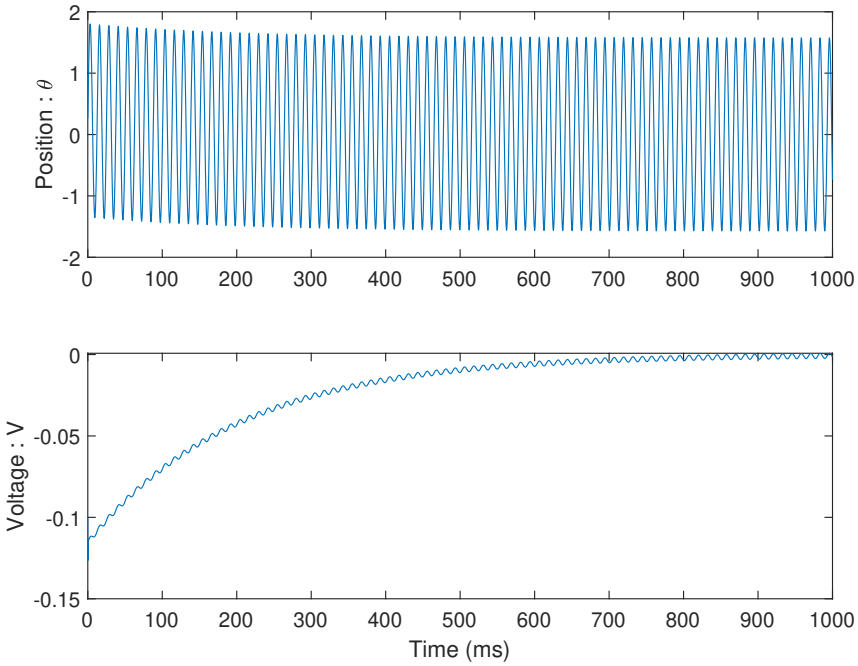

Figure 4.2: Voltage response of rotation in single node

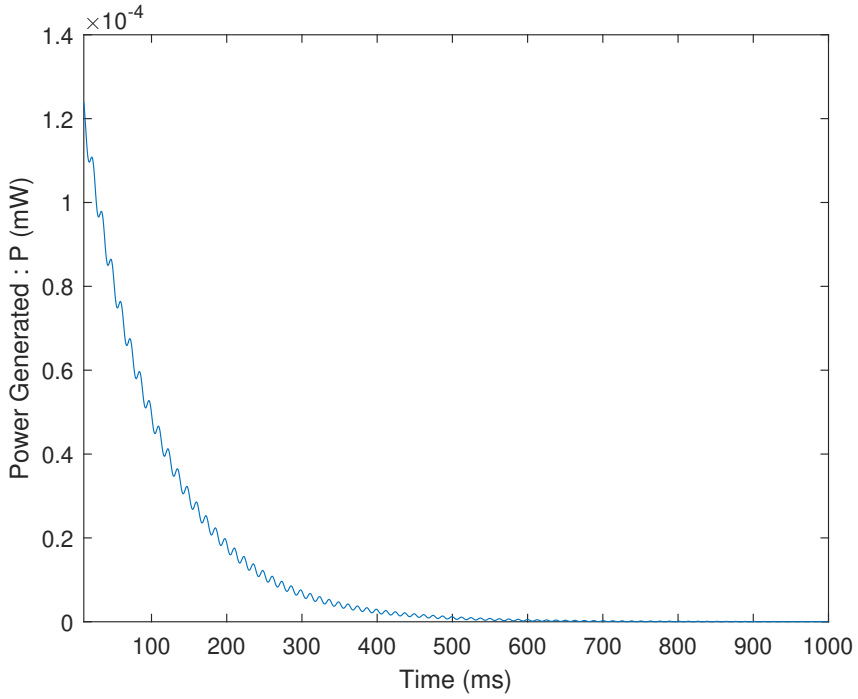

Figure 4.3: Power generated in rotation of a single node

4.2 Multi Node Model

In the multi node model, each rod is connected to one another and the origin O as shown in Fig. 4.4. This section explores the mathematical modeling of the multi node model for two cases: constant intrinsic angle and variable intrinsic angle.

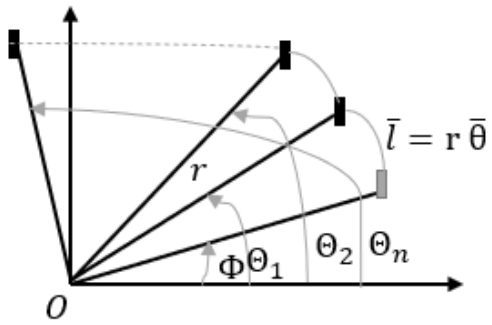

Figure 4.4: Multiple Node Bending

4.2.1 Dynamic Modeling

4.2.1.1 Modeling with Constant Intrinsic Angle

In this scenario, the intrinsic angle $\bar{\theta}$, remains constant. Each link rotates in response to the input vibration, $u = \left[\phi\ \dot{\phi}\right]$. The equations of motion with small angle approximation are given below:

$$
\begin{aligned}
I\ddot{\theta}_1 &= -\kappa\left(\theta_1 - \bar{\theta} - \phi\right) + \kappa\left(\theta_2 - \bar{\theta} - \theta_1\right) \\
&\quad - \mathcal{B}\left(\dot{\theta}_1 - \dot{\phi}\right) + \mathcal{B}\left(\dot{\theta}_2 - \dot{\theta}_1\right) - \alpha V_1 \\
\alpha r\left(\dot{\theta}_1 - \dot{\phi}\right) - C_p\dot{V}_1 &= \frac{V_1}{R} \\
I\ddot{\theta}_i &= -\kappa\left(\theta_i - \bar{\theta} - \theta_{i-1}\right) + \kappa\left(\theta_{i+1} - \bar{\theta} - \theta_i\right) \\
&\quad - \mathcal{B}\left(\dot{\theta}_i - \dot{\theta}_{i-1}\right) + \mathcal{B}\left(\dot{\theta}_{i+1} - \dot{\theta}_i\right) - \alpha V_i \\
\alpha r\left(\dot{\theta}_i - \dot{\theta}_{i-1}\right) - C_p\dot{V}_i &= \frac{V_i}{R} \\
I\ddot{\theta}_n &= -\kappa\left(\theta_n - \bar{\theta} - \theta_{n-1}\right) - \mathcal{B}\left(\dot{\theta}_n - \dot{\theta}_{n-1}\right) - \alpha V_n \\
\alpha r\left(\dot{\theta}_n - \dot{\theta}_{n-1}\right) - C_p\dot{V}_n &= \frac{V_n}{R}
\end{aligned}
\tag{4.5}
$$

$$
\begin{aligned}
\ddot{\theta}_1 &= \frac{1}{I}\left(-2\kappa\theta_1 + \kappa\theta_2 - 2\mathcal{B}\dot{\theta}_1 + \mathcal{B}\dot{\theta}_2 - \alpha V_1 + \kappa\phi + \mathcal{B}\dot{\phi}\right) \\
\dot{V}_1 &= \frac{1}{C_P}\left(\alpha r\left(\dot{\theta}_1 - \dot{\phi}\right) - \frac{V_1}{R}\right) \\
\ddot{\theta}_i &= \frac{1}{I}\left(-2\kappa\theta_i + \kappa\theta_{i-1} + \kappa\theta_{i+1} - 2\mathcal{B}\dot{\theta}_i + \mathcal{B}\theta_{i-1} + \mathcal{B}\theta_{i+1} - \alpha V_i\right) \\
\dot{V}_i &= \frac{1}{C_p}\left(\alpha r\left(\dot{\theta}_i - \dot{\theta}_{i-1}\right) - \frac{V_i}{R}\right) \\
\ddot{\theta}_n &= \frac{1}{I}\left(-\kappa\theta_n + \kappa\theta_{n-1} + \kappa\bar{\theta} - \mathcal{B}\dot{\theta}_n + \mathcal{B}\dot{\theta}_{n-1} - \alpha V_n\right) \\
\dot{V}_n &= \frac{1}{C_p}\left(\alpha r\left(\dot{\theta}_n - \dot{\theta}_{n-1} - \frac{V_n}{R}\right)\right)
\end{aligned}
\tag{4.6}
$$

4.2.1.2 Modeling with Varying Intrinsic Angle

In the case of varying intrinsic angles, the intrinsic angles $\bar{\theta}_1, \bar{\theta}_2, \ldots, \bar{\theta}_n$, vary in response to a travelling wave motion. The equations of motion for this scenario are

$$\begin{aligned}
I\ddot{\theta}_1 &= -\kappa\left(\theta_1 - \bar{\theta}_1 - \phi\right) + \kappa\left(\theta_2 - \bar{\theta}_2 - \theta_1\right) \\
&\quad - \mathcal{B}\left(\dot{\theta}_1 - \dot{\bar{\theta}}_1 - \dot{\phi}\right) + \mathcal{B}\left(\dot{\theta}_2 - \dot{\bar{\theta}}_2 - \dot{\theta}_1\right) - \alpha V_1 \\
\alpha r\left(\dot{\theta}_1 - \dot{\phi}\right) - C_p\dot{V}_1 &= \frac{V_1}{R} \\
I\ddot{\theta}_i &= -\kappa\left(\theta_i - \bar{\theta}_i - \theta_{i-1}\right) + \kappa\left(\theta_{i+1} - \bar{\theta}_{i+1} - \theta_i\right) \\
&\quad - \mathcal{B}\left(\dot{\theta}_i - \dot{\bar{\theta}}_i - \dot{\theta}_{i-1}\right) + \mathcal{B}\left(\dot{\theta}_{i+1} - \dot{\bar{\theta}}_{i+1} - \dot{\theta}_i\right) - \alpha V_i \\
\alpha r\left(\dot{\theta}_i - \dot{\theta}_{i-1}\right) - C_p\dot{V}_i &= \frac{V_i}{R} \\
I\ddot{\theta}_n &= -\kappa\left(\theta_n - \bar{\theta}_n - \theta_{n-1}\right) - \mathcal{B}\left(\dot{\theta}_n - \dot{\bar{\theta}}_n - \dot{\theta}_{n-1}\right) - \alpha V_n \\
\alpha r\left(\dot{\theta}_n - \dot{\theta}_{n-1}\right) - C_p\dot{V}_n &= \frac{V_n}{R}
\end{aligned} \tag{4.7}$$

Simplifying the above Equation gives

$$
\begin{aligned}
\ddot{\theta}_1 &= \frac{1}{I}\left(-2\kappa\theta_1 + \kappa\theta_2 + \kappa\bar{\theta}_1 - \kappa\bar{\theta}_2 - 2\mathcal{B}\dot{\theta}_1 + \mathcal{B}\dot{\theta}_2 + \mathcal{B}\dot{\bar{\theta}}_1 - \mathcal{B}\dot{\bar{\theta}}_2 - \alpha V_1 + \kappa\phi + \mathcal{B}\dot{\phi}\right) \\
\dot{V}_1 &= \frac{1}{C_P}\left(\alpha r\left(\dot{\theta}_1 - \dot{\phi}\right) - \frac{V_1}{R}\right) \\
\ddot{\theta}_i &= \frac{1}{I}\left(-2\kappa\theta_i + \kappa\theta_{i-1} + \kappa\theta_{i+1} + \kappa\bar{\theta}_i - \kappa\bar{\theta}_{i+1} - 2\mathcal{B}\dot{\theta}_i + \mathcal{B}\theta_{i-1} + \mathcal{B}\theta_{i+1} + \mathcal{B}\dot{\bar{\theta}}_i - \mathcal{B}\dot{\bar{\theta}}_{i+1} - \alpha V_i\right) \\
\dot{V}_i &= \frac{1}{C_p}\left(\alpha r\left(\dot{\theta}_i - \dot{\theta}_{i-1}\right) - \frac{V_i}{R}\right) \\
\ddot{\theta}_n &= \frac{1}{I}\left(-\kappa\theta_n + \kappa\theta_{n-1} + \kappa\bar{\theta} - \mathcal{B}\dot{\theta}_n + \mathcal{B}\dot{\theta}_{n-1} + \mathcal{B}\dot{\bar{\theta}}_n - \alpha V_n\right) \\
\dot{V}_n &= \frac{1}{C_p}\left(\alpha r\left(\dot{\theta}_n - \dot{\theta}_{n-1} - \frac{V_n}{R}\right)\right)
\end{aligned}
\tag{4.8}
$$

4.2.2 Energy Generated

The output power of the system is calculated using the Equation 3.20. The output power for constant intrinsic angle and varying intrinsic is shown in the Fig. 4.5. It can be observed that after the initial noise subsides, the output power generated in the case when the intrinsic length is varied is higher. But this output power is lower than the case of stretching of the piezoelectric devices.

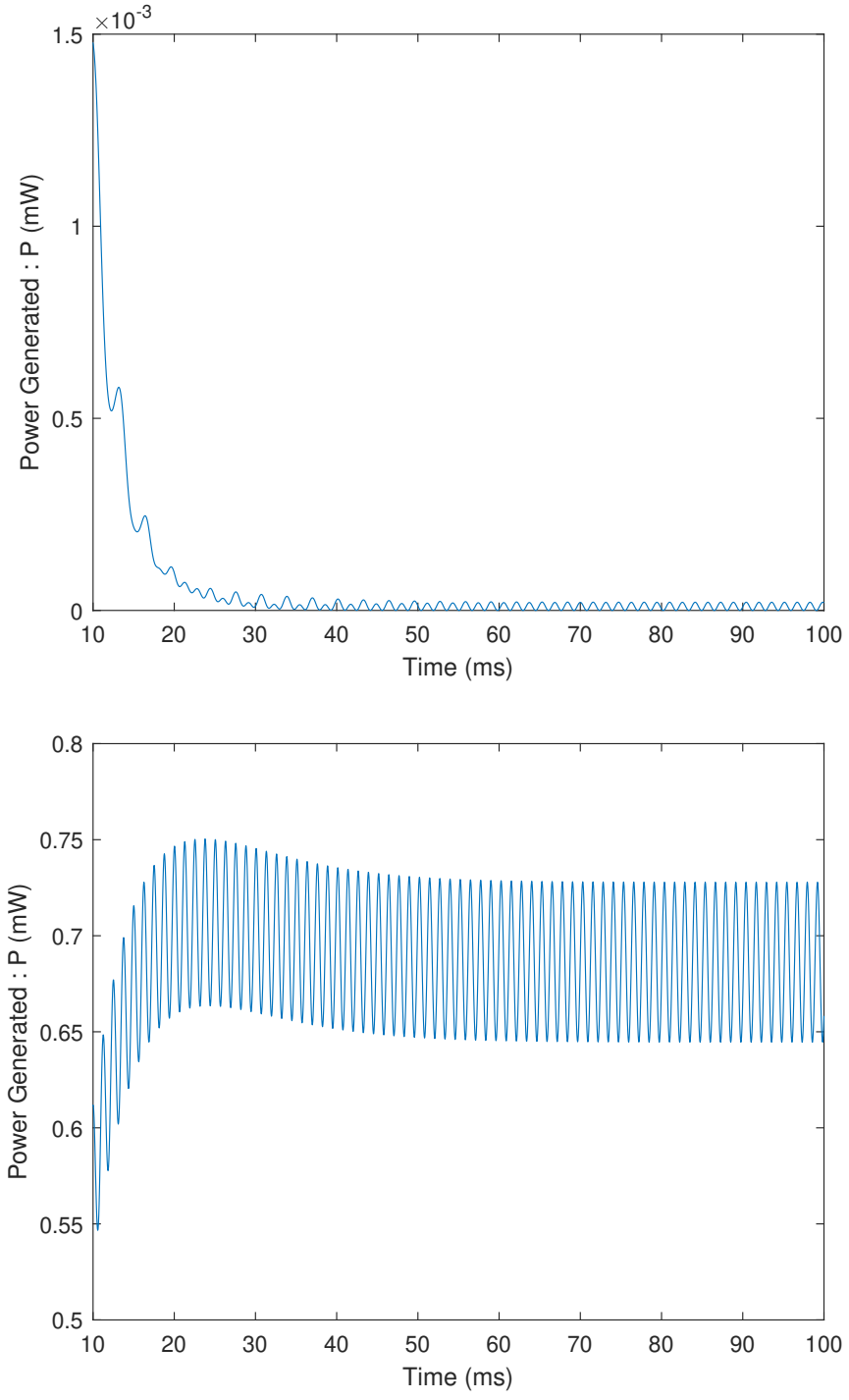

Figure 4.5: Output power for constant intrinsic angle and varying intrinsic angle

4.3 Modeling Response for Different Forcing

The models developed in section 4.2.1.2 and 4.2.1.1 are simulated using sinusoidal input. The result of the simulation is discussed in this section. The series voltage is found by:

$$V_s = \sum_{i=1}^{n} V_i \tag{4.9}$$

4.3.1 Responses for Constant Intrinsic Angle

The model developed in section Sec. 4.2.1.2 is simulated using sinusoidal input. It can be noted that even in series connection of 10 piezoelectric devices, the generated voltage is low. Though the response looks similar to the case of stretching, but since, rotation produces less strain as compared to stretching, the overall voltage output is low. But compared to the case of stretching, the output is more stable. Hence, a higher strain though results in higher voltage, but it compromises the stability of the system.

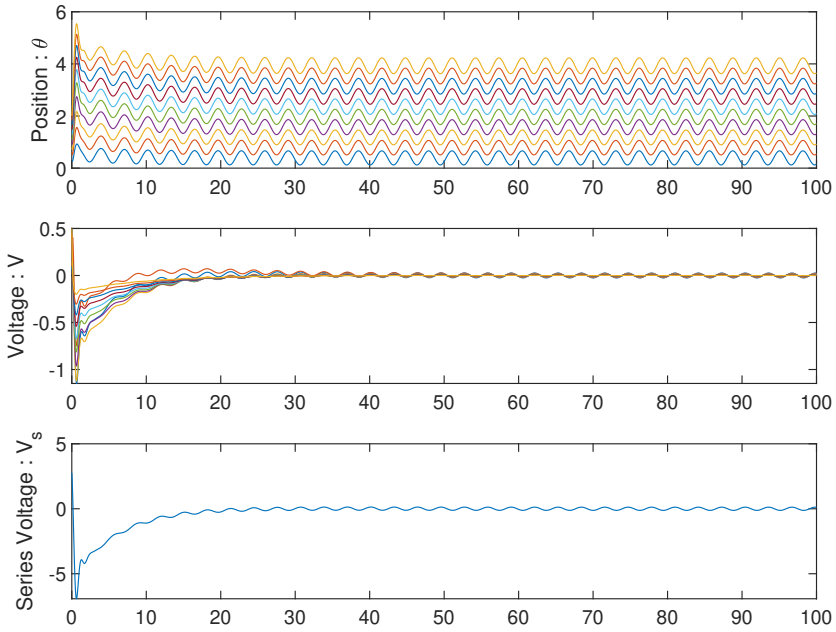

Figure 4.6: Angular rotation, generated voltage and series voltage for rotation of 10 nodes when intrinsic angle remains constant

4.3.2 Responses for Variable Intrinsic Angle

The model developed in section Sec. 4.2.1.1 is simulated using sinusoidal input. Here, similar to the case of of varying intrinsic length in stretching, the angles are out of phase with each other, hence the voltage produced is out of phase. This results in higher output voltage V_s. Though the output is lesser when compared to stretching, it is higher than the output produced when the intrinsic length remains constant.

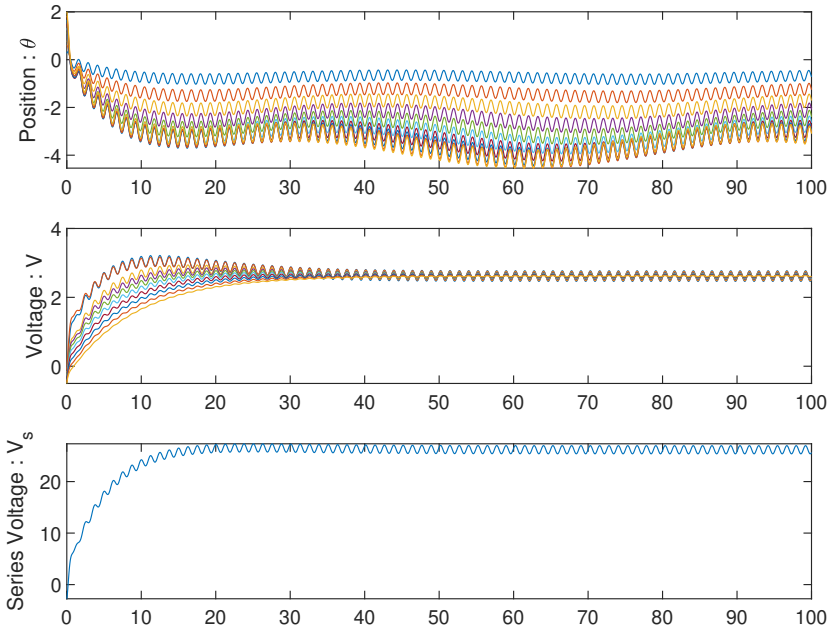

Figure 4.7: Angular rotation, generated voltage and series voltage for rotation of 10 nodes when intrinsic angle is varied

Chapter 5: Conclusion

Every progress comes with a price. The progress made in robotic and automation have made life easier for humans, but these come with a heavy price paid by the environment. The use of wireless non-renewable power sources like batteries has resulted in unimaginable solid waste. Hence, recent decades have seen a rise in alternative power sources.

The alternative power sources provide a better solution for the environment and effectively reduce the cost of replaceable batteries and recharging of batteries. Piezoelectric energy harvesting provides a good source of alternative energy.

In the case of soft robotics, harvesting energy using flexible piezoelectric polymers reduces the bulk power requirement. It retains the robot's flexibility and increases the operation time by reducing the need for recharging the power source.

5.1 Summary of Contributions

The primary contribution of this thesis is deriving the mathematical model for energy generated by piezoelectric devices. The lumped parameter model of piezoelectricity provides an efficient and easy method of analyzing the behavior of the energy harvesting system vibrating linearly. This model is expanded to include multiple piezoelectric devices and the rotation of the devices in this thesis.

The lumped parameter model considers a tip mass mounted of a spring and damper with a vibrating base. Chapter 4 looks into the case when multiple devices are coupled mechanically and stretched linearly. Two models depicting two cases: no intrinsic vibration of links and another with intrinsic vibration of strings is developed and simulated. This model is further expanded to the case of solid rods instead of tip mass in chapter 5.

The work extensively looks into the voltage generated and output power in the cases described.

5.2 Suggestion for Ongoing and Future Work

In this thesis, two cases of piezoelectric energy harvesting are explored. The results from these two cases can be further expanded to soft, segmented robots. The model of soft, segmented robot developed in [17] can be used for this purpose. This would provide a way to implement the developed piezoelectric models with snake-like soft robots.

The state-space model suggested below incorporates piezoelectric energy harvesting in a soft, segmented robot:

$$
\begin{aligned}
\dot{q} &= v \\
\dot{v} &= -M^{-1}\left(\frac{\partial E_t}{\partial q} + \alpha V + F_{ext}\right) \\
\dot{\bar{\kappa}} &= B_k u_k \\
\dot{\bar{l}} &= B_l u_l \\
\dot{V} &= -\mathbf{A}v - \frac{V}{R}
\end{aligned}
\tag{5.1}
$$

Where, $q = (x_1, y_1, \ldots, x_N, y_N)^{'}$ represents the Cartesian coordinates of all the nodes of the soft robot and $v = (\dot{x}_1, \dot{y}_1, \ldots, \dot{x}_N, \dot{y}_N)$ represents the node velocities. $\bar{\kappa}$ represents the intrinsic curvature and $\bar{l}$ represents the intrinsic length of each edge. The matrix $\mathbf{A}$ is defined by the following matrix:

$$\mathbf{A} = \begin{bmatrix} \alpha & -\alpha & 0 & \ldots & 0 \\ 0 & \alpha & -\alpha & \ldots & 0 \\ & & \ldots & & \\ 0 & \ldots & 0 & \alpha & -\alpha \end{bmatrix} \tag{5.2}$$

Analyzing the results for the above equations can provide some interesting results.

Bibliography

[1] Alper Erturk and Daniel J. Inman. *Piezoelectric Energy Harvesting*. 2011.

[2] Rafael Tavares and Michael Ruderman. On Energy Harvesting Using Piezoelectric Transducer with Two-Port Model under Force Excitation. *Proceedings - 2019 IEEE International Conference on Mechatronics, ICM 2019*, pages 414–419, 2019.

[3] Guo-Ying Gu, Li-Min Zhu, Chun-Yi Su, Han Ding, and Sergej Fatikow. Modeling and control of piezo-actuated nanopositioning stages: A survey. *IEEE Transactions on Automation Science and Engineering*, 13(1):313–332, 2016.

[4] Corina Covaci and Aurel Gontean. Piezoelectric energy harvesting solutions: A review. *Sensors (Switzerland)*, 20(12):1–37, 2020.

[5] Jingjing Zhao and Zheng You. A shoe-embedded piezoelectric energy harvester for wearable sensors. *Sensors (Switzerland)*, 14(7):12497–12510, 2014.

[6] Liya Zhao, Lihua Tang, and Yaowen Yang. Comparison of modeling methods and parametric study for a piezoelectric wind energy harvester. *Smart Materials and Structures*, 22(12), 2013.

[7] Abdessattar Abdelkefi and Mehdi Ghommem. Piezoelectric energy harvesting from morphing wing motions for micro air vehicles. *Theoretical and Applied Mechanics Letters*, 3(5):052004, 2013.

[8] Xiaobiao Shan, Rujun Song, Bo Liu, and Tao Xie. Novel energy harvesting: A macro fiber composite piezoelectric energy harvester in the water vortex. *Ceramics International*, 41(S1):S763–S767, 2015.

[9] Mohsen Safaei, Henry A. Sodano, and Steven R. Anton. A review of energy harvesting using piezoelectric materials: State-of-the-art a decade later (2008-2018). *Smart Materials and Structures*, 28(11), 2019.

[10] Sibel Akkaya Oy. A Design of mass-spring type piezoelectric energy harvesting. *Scientia Iranica*, 0(0):0–0, 2020.

[11] Guang Qing Wang and Yue Ming Lu. An improved lumped parameter model for a piezoelectric energy harvester in transverse vibration. *Shock and Vibration*, 2014, 2014.

[12] Satu Kärki and Jukka Lekkala. A lumped-parameter transducer model for piezoelectric and ferroelectret polymers. *Measurement: Journal of the International Measurement Confederation*, 45(3):453–458, 2012.

[13] Srimanta Baishya, Debarun Borthakur, Richik Kashyap, and Amitabh Chatterjee. A High Precision Lumped Parameter Model for Piezoelectric Energy Harvesters. *IEEE Sensors Journal*, 17(24):8350–8355, 2017.

[14] Canan Dagdeviren, Pauline Joe, Ozlem L. Tuzman, Kwi Il Park, Keon Jae Lee, Yan Shi, Yonggang Huang, and John A. Rogers. Recent progress in flexible and stretchable piezoelectric devices for mechanical energy harvesting, sensing and actuation. *Extreme Mechanics Letters*, 9:269–281, 2016.

[15] Eleni Kelasidi, Pål Liljebäck, Kristin Y. Pettersen, and Jan Tommy Gravdahl. Integral line-of-sight guidance for path following control of underwater snake robots: Theory and experiments. *IEEE Transactions on Robotics*, 33(3):610–628, 2017.

[16] Travis Burch, John P. Lathrop, William L. Scott, and Derek A. Paley. Feedback Control of a Soft Swinging Appendage. *2020 3rd IEEE International Conference on Soft Robotics, RoboSoft 2020*, (1):621–626, 2020.

[17] William L. Scott, Prateek Jaya Prakash, and Derek A. Paley. Distributed control of a planar discrete elastic rod model for caterpillar-inspired locomotion. *ASME 2019 Dynamic Systems and Control Conference, DSCC 2019*, 3, 2019.

[18] H Araya, L Li, et al. Development of a creeping locomotion snake robot. *International Journal of Robotics and Automation*, (2003067355442), 2002.

[19] Li Chen, Yuechao Wang, Shugen Ma, and Bin Li. Analysis of traveling wave locomotion of snake robot. 1:365–369, 2003.

[20] Xinda Qi, Hongyang Shi, Thassyo Pinto, and Xiaobo Tan. A novel pneumatic soft snake robot using traveling-wave locomotion in constrained environments. *IEEE Robotics and Automation Letters*, 5(2):1610–1617, 2020.

[21] Sushanta Kundu and Harshal B. Nemade. Modeling and Simulation of a Piezoelectric Vibration Energy Harvester. *Procedia Engineering*, 144:568–575, 2016.

[22] Richard M Martin. Physical Review B Volume 5, Number 4 Piezoelectricity. Technical report, 1972.

[23] Y. C. Shu and I. C. Lien. Analysis of power output for piezoelectric energy harvesting systems. *Smart Materials and Structures*, 15(6):1499–1512, 2006.

[24] Shashank Priya and Daniel J. Inman. Energy harvesting technologies. *Energy Harvesting Technologies*, pages 1–517, 2009.

[25] W.L. Hosch. Descartes's rule of signs — mathematics — Britannica. *Encyclopædia Britannica*, 2011.